R.T.J McAteer **CUME #397** **April 2015**

This CUME is based on the accompanying paper by Tian et al, 2014, Science, 346, 1155711. It is not important to read the paper in intricate detail. Instead you should spend no more than 10 minutes reading the paper, and 5 minutes familiarizing yourself with the figures, before beginning the exam.

There are 100 total points available. A grade of 70% is *expected* to be a passing grade. There are 4 questions (1 has 15 points, 2 has 25 points, 3 has 20 points, and 4 has 40 points). Keep careful time management to ensure you have sufficient time for all the questions.

Calculators are only to be used for calculations.
Show all work for full points.
Attempt all parts of all questions.
Take a new page for each part of each question.

Some Constants and Equations.

1AU = 215 Solar radii
1 Solar radius = 6.95×10^5 km
1 arcsec = 4.85×10^{-6} radians
By definition, 1 Mx cm^{-2} =1 G
Bohr magneton, $U_B = 9.27 \times 10^{-21}$ ergs G-1
Planck constant, $h = 6.63 \times 10^{-27}$ erg s
Speed of light, $c = 3 \times 10^8$ m s^{-1}
Ampere's law, $\nabla \times B = \mu_o J$
By conversion, 1 Joule = 10^7 ergs
Boltzmann constant, $k_B = 1.38 \times 10^{-16}$ erg K^{-1}
Energy gained by an electron across 1 volt, 1eV $= 1.6 \times 10^{-19}$ J
Mass of a proton, $m_p = 1.67 \times 10^{-24}$ g

1: This question asks you calculate the velocity of the jets in Figure 1.

(i) Using basic geometry, show that that the angle subtended by the Sun is 1920 arc sec **5 points**

(ii) Use figure 1 to show that the velocity of the jet is consistent with the stated value of 206 km s^{-1}. **10 points**

2: This question asks you to discuss the data presented in Figure 2

(i) The IRIS data in Figure 2 are stated to have a spatial resolution of 250km. Calculate the diameter of the IRIS telescope mirror. **10 points**

(ii) The third ionization potential of Si is 33.5ev. Show this is consistent with a Transition Region temperature of 10^5 K. **10 points**

(iii) The chromospheric Fraunhofer lines appear almost exclusively in absorption. Why do the Transition Region far-UV lines appear in emission, and, as such, what is the likely excitation mechanism for these far-UV lines? **5 points**

3.The question probes your knowledge of spectroscopic techniques as applied to Figure 3D and 3E.

(i) Assume the observed Gaussian line profiles are probing a combination of two Gaussian profiles - thermal and non-thermal broadening. The FWHM of such a Gaussian profile is about 2.4σ. Thermal broadening is determined as $v_{th} = ((2kT) / (m_{ion}))^{0.5}$ where the mass of the Silicon Ion is 4.6 x 10^{-23} g. Use Figure 3D to calculate the non-thermal velocity at location 2 and show this is greater than the value quoted in the abstract.

15 points

(ii) In this article, the authors attribute the non-thermal component to (transverse) Alfven waves (bottom of page 3 and top of page 4). Discuss two contributions to the observed line widths in Figure 3 that have we neglected in 3(i) above. **5 points**

4. This question addresses the conclusion that these jets provide sufficient mass for the solar wind

(i) Show that the general equation for mass loss rate $\dot{M}$, given below, through a sphere is dimensionally consistent. **5 points**

$$\dot{M} = \text{(Surface area of sphere) x (mass density) x (velocity) } f_t \text{ x } f_s$$

where f_s is a dimensionless space-filling factor and f_t is a dimensionless time-filling factor, both of which will between 0 and 1.

(ii) Comment on why the authors require f_s and f_t ,and use the values provided (Figure 1 and midway thru page 3) to show a time filling factor of about 10% is appropriate.

15 points

(iii) Using values provided in Fig 1 to calculate the stated mass loss rate of 2–30 x 10^{12} g s^{-1}. You can assume a space filling factor of about 0.1% to 1% for these jets over the solar surface, a typical jet electron number density of n_e=10^{11} cm^{-3} , and a reasonable coronal Helium abundance of 5% (neglecting all other metals). **10 points**

(iv) The solar wind density measured at Earth is 5 protons cm^{-3}, with a solar wind velocity of about 600 km s^{-1} . Show this results in a flux of about 5 x 10^{-16} g s^{-1} cm^{-2} at Earth, and hence calculate an estimate for the total solar wind mass rate which is 2-24 lower than provided by these jets, as stated in the paper. **10 points**

(1)

1) From constants provided, Sun is 1 $R_\odot$ at a distance of 215 $R_\odot$

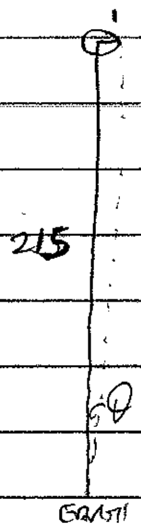

From geometry

$$\frac{\theta}{360} = \frac{R_\odot}{2\pi(215 R_\odot)}$$

$$= \frac{1}{2\pi(215)}$$

$$\theta = \frac{360}{(2\pi)(215)}$$

$$= 0.266^\circ$$

$$= 960''$$

Angle subtended by Sun is $2 \times 960 = 1920''$

OR SIMPLY

$\tan\theta = \frac{1}{215}$

$\Rightarrow \theta = 0.266^\circ$

(1)

ii)

Fig 1B is a space-time plot.
Velocity is just the gradient of the line as marked

$$v = \frac{d}{t} = \frac{10''}{250 - 215}$$

From i) and using constants provided

$$960'' = 6.95 \times 10^5 \text{ km at the Sun}$$

so,
$$v = \frac{6.95 \times 10^5}{96 \times 35}$$

$$= \left(\frac{6.95}{9.6 \times 3.5}\right) \times 10^{5-1-1}$$

$$\approx \frac{7}{35} \times 10^3$$

$$\sim 0.2 \times 10^3$$

$$\sim 200 \text{ km s}^{-1}$$

value provided in Fig 1(b) is 206 kms^{-1}

(2)

(i) From basic knowledge of telescopes

$$\theta_{res} = 1.22 \frac{\lambda}{D}$$

$$D = \frac{1.22\lambda}{\theta_{res}}$$

Data resolution = 250 km

From before $960''$ = 6.95×10^5 km

$$\frac{(2.5\times10^2)(9.6\times10^2)''}{6.95\times10^5} = 250 \text{ km}$$

$$\frac{2.5\times9.6}{6.95}\times10^{2+2-5} = 250 \text{ km}$$

25/7

$7\times3=21$

$$3.5\times10^{-1} = 250 \text{ km}$$

θ_{res} is half of this value $\Rightarrow 1.8\times10^{-1}$ ''

From constants provided $\theta_{res} \sim (1.8\times10^{-1})(4.85\times10^{-6})$ radians

$\sim 8.5\times10^{-7}$ radians

$$D = \frac{(1.22)(1330\times10^{-10})}{8.5\times10^{-7}}$$

$$\sim\left(\frac{1.2\times1.3}{8.5}\right)\times10^{-10+7}$$

$$\sim \frac{1}{5}\times10^{-3}$$

$\sim 0.2 \times 10^{-3}$

~ 20 cm

2

(ii) Ionisation potential is energy required to free the 2nd electron

$$E \sim k_B T$$

Careful with units

$$(33.5)(1.6 \times 10^{-19}) = \frac{(1.4 \times 10^{-16})}{10^7} T$$

$$T = \left(\frac{3.35 \times 1.6}{1.4}\right) \times 10^{1-19+7+16}$$

$$\sim 3.5 \times 10^5 \ K$$

agrees with value of 10^5 K provided in the paper and is between chromospheric (5×10^3 K) and coronal (10^6 K) temperatures

(2)

iii) UV spectral emission requires high temperatures, hence TR.

At ~~UV~~ (far)-UV wavelengths the flux from photospheric continuum is low

In chromosphere temperature is lower and background is higher, so lines are in absorption

∴ Because of low flux, radiative excitation does not occur.
High T allows for collisional excitation and emission upon returning to ground state

(3)

(i)

$$\Delta v = \sqrt{v_{TH}^2 + v_{NT}^2}$$

For the silicon ion, choose $T \sim 10^5$ K

$$v_{TH}^2 = \frac{2(1.38\times10^{-16})(10^5)}{4.6\times10^{-23}}$$

$$\simeq 0.6 \times 10^{-16+5+23}$$

$$\simeq 60 \times 10^{10} \ cm^2 s^{-2}$$

~~$v \simeq 0.7 \times 10^{5} \ cm\,s^{-1}$~~

$$v \sim 7 \times 10^5 \ cm\,s^{-1}$$

$$\sim 7 \ km\,s^{-1}$$

From Figure 3, location 2, FWHM ~ 70 km s^{-1}

$\Delta v \sim \frac{70}{2.4} \sim 29$ km s^{-1}

$$29^2 = 7^2 + v_{NT}^2$$

$$\Rightarrow v_{NT} \sim 28 \ km\,s^{-1}$$

③

(ii) From the article $v_{nT} \sim 21$ km s^{-1}

We have not accounted for instrumental broadening in our Δv equation

$$v = \sqrt{v_T^2 + v_{nT}^2 + v_{inst}^2}$$

is the better equation

In location 1 there is also an upflow (field aligned flow) that makes it even broader.

Allowed Also microturbulence?
pressure?

(4)

(i)

$$\dot{m} = (L^2)\left(\frac{M}{L^3}\right)\left(\frac{L}{T}\right)$$

$$= \frac{M}{T}$$

or student can use any unit system for M, L, T

(4)

(ii) From the article

Figure 1 → $\tau \sim 50$ secs

Repeat time $\sim$ 2 - 15 minutes

$$\Rightarrow F_t \sim \frac{50}{8 \times 60} \sim \frac{50}{480} \sim 0.1$$

$$F = \frac{\tau}{t_r} \quad \tau / F \quad \Rightarrow t_r$$

~~Are~~ Jets are neither space or time continuous
Jets do not fill all the surface
Jets do not flow all the time

(4)

(iii)

$$\dot{M} = (4\pi R_s)^2 (\rho)(v) \; f_s f_t$$

From

Calculate $\rho = n_e \mu m_p$

At 5%, 95% H, $\mu \sim \frac{(95 \times 1) + (5 \times 4)}{100}$

~ 1.15

$$\Rightarrow \rho = (10^{11})(1.15)(1.67 \times 10^{-24})$$

$$\cong 2 \times 10^{11-24}$$

$$\cong 2 \times 10^{-13} \; g/cm^3$$

$$\dot{M} = 4\pi (6.95 \times 10^{10})^2 (2 \times 10^{-13})(150 \times 10^{5})(0.1)(0.001)$$

$$\sim (1.2 \times 7^2 \times 2 \times 1.5) \times 10^{1+20-13+7-1-3}$$

$$\sim 20 \times 10^{11} \; g \, s^{-1}$$

(1.4 × 10^{12})

$$\sim 2 \times 10^{12} \; g \, s^{-1}$$

(iv) At Earth, Flux $= \rho v$ $\left[\frac{m}{L^3}\frac{L}{T} = m T^{-1} L^{-2}\right.$

$\rho v : \frac{g}{cm^3}\frac{cm}{s}$

$$= 5(1.67\times10^{-24})(600\times10^5)$$

$$\simeq 5\times1.67\times6 \times10^{-24+7}$$

$$\sim 50 \times10^{-17} \; g\,s^{-1}\,cm^{-2}$$

$$\sim 5 \times10^{-16} \; g\,s^{-1}\,cm^{-2}$$

To convert to mass loss ($g\,s^{-1}$), multiply by the ~~size~~ area of a sphere, radius 1 AU

$$\dot{m} = (4\pi R^2)\,(5\times10^{-16})$$

$$= 4\pi\left((2.15\times10^2)\times(6.95\times10^{10})\right)^2 (5\times10^{-16})$$

$$\simeq (1.2\times1.5^2\times5)\times10^{1+13+13-16}$$

$$\simeq 12\times10^{11} \; g\,s^{-1}$$

$$\sim 1.2\times10^{12} \; g\,s^{-1}$$

SOLAR PHYSICS

Prevalence of small-scale jets from the networks of the solar transition region and chromosphere

H. Tian,[1]* E. E. DeLuca,[1] S. R. Cranmer,[1] B. De Pontieu,[2] H. Peter,[3] J. Martínez-Sykora,[2,4] L. Golub,[1] S. McKillop,[1] K. K. Reeves,[1] M. P. Miralles,[1] P. McCauley,[1] S. Saar,[1] P. Testa,[1] M. Weber,[1] N. Murphy,[1] J. Lemen,[2] A. Title,[2] P. Boerner,[2] N. Hurlburt,[2] T. D. Tarbell,[2] J. P. Wuelser,[2] L. Kleint,[2,4] C. Kankelborg,[5] S. Jaeggli,[5] M. Carlsson,[6] V. Hansteen,[6] S. W. McIntosh[7]

As the interface between the Sun's photosphere and corona, the chromosphere and transition region play a key role in the formation and acceleration of the solar wind. Observations from the Interface Region Imaging Spectrograph reveal the prevalence of intermittent small-scale jets with speeds of 80 to 250 kilometers per second from the narrow bright network lanes of this interface region. These jets have lifetimes of 20 to 80 seconds and widths of ≤300 kilometers. They originate from small-scale bright regions, often preceded by footpoint brightenings and accompanied by transverse waves with amplitudes of ~20 kilometers per second. Many jets reach temperatures of at least $\sim 10^5$ kelvin and constitute an important element of the transition region structures. They are likely an intermittent but persistent source of mass and energy for the solar wind.

The Sun continuously emits ionized particles into interplanetary space in the form of the solar wind. A challenging investigation has now carried on for almost 50 years to understand where the solar wind originates and how it is accelerated (*1*, *2*). Dark regions in coronal images indicate the coronal holes that are the commonly accepted large-scale source regions of the high-speed solar wind. However, identifying precise origin sites within coronal holes requires high-resolution observations of the chromosphere and transition region (TR), a complex interface between the relatively cool photosphere ($\sim 6 \times 10^3$ K) and hot corona ($\sim 10^6$ K). The mass and energy that ultimately feed the solar wind must pass through this region.

The dominant emission features in this interface region are the network structures that appear as narrow bright lanes enclosing dark cells, with sizes of ~20,000 km in radiance images of emission lines (*3*). The network lanes (networks thereafter) are believed to be locations of strong magnetic fluxes originating from the boundaries of convection cells with similar sizes in the photosphere. Previous observations of coronal holes with the Solar Ultraviolet Measurements of Emitted Radiation (SUMER) instrument (*4*) onboard the Solar and Heliospheric Observatory (SOHO) revealed Doppler blue shifts of 5 to 10 km s^{-1} for emission lines formed in the upper TR (*5*). They were interpreted as signatures of the nascent solar wind guided by funnellike magnetic structures originating from the networks (*6*).

Recent analyses revealed weak blue wing enhancements in profiles of emission lines formed in the TR (*7*, *8*). These weak enhancements indicate the possible presence of a plasma component flowing upward with speeds of 50 to 100 km s^{-1}, which may provide heated mass to the solar wind (*8*). It has been difficult to test this proposed idea without direct imaging of such TR upflows on the solar disk, although moderate-resolution observations have revealed signatures

[1]Harvard-Smithsonian Center for Astrophysics, 60 Garden Street, Cambridge, MA 02138, USA. [2]Lockheed Martin Solar and Astrophysics Laboratory, 3251 Hanover Street, Organization A021S, Building 252, Palo Alto, CA 94304, USA. [3]Max Planck Institute for Solar System Research, Justus-von-Liebig-Weg 3, 37077 Göttingen, Germany. [4]Bay Area Environmental Research Institute, 596 1st Street West, Sonoma, CA 95476, USA. [5]Department of Physics, Montana State University, Post Office Box 173840, Bozeman, MT 59717, USA. [6]Institute of Theoretical Astrophysics, University of Oslo, Post Office Box 1029, Blindern, 0315 Oslo, Norway. [7]High Altitude Observatory, National Center for Atmospheric Research, Post Office Box 3000, Boulder, CO 80307, USA.
*Corresponding author. E-mail: hui.tian@cfa.harvard.edu

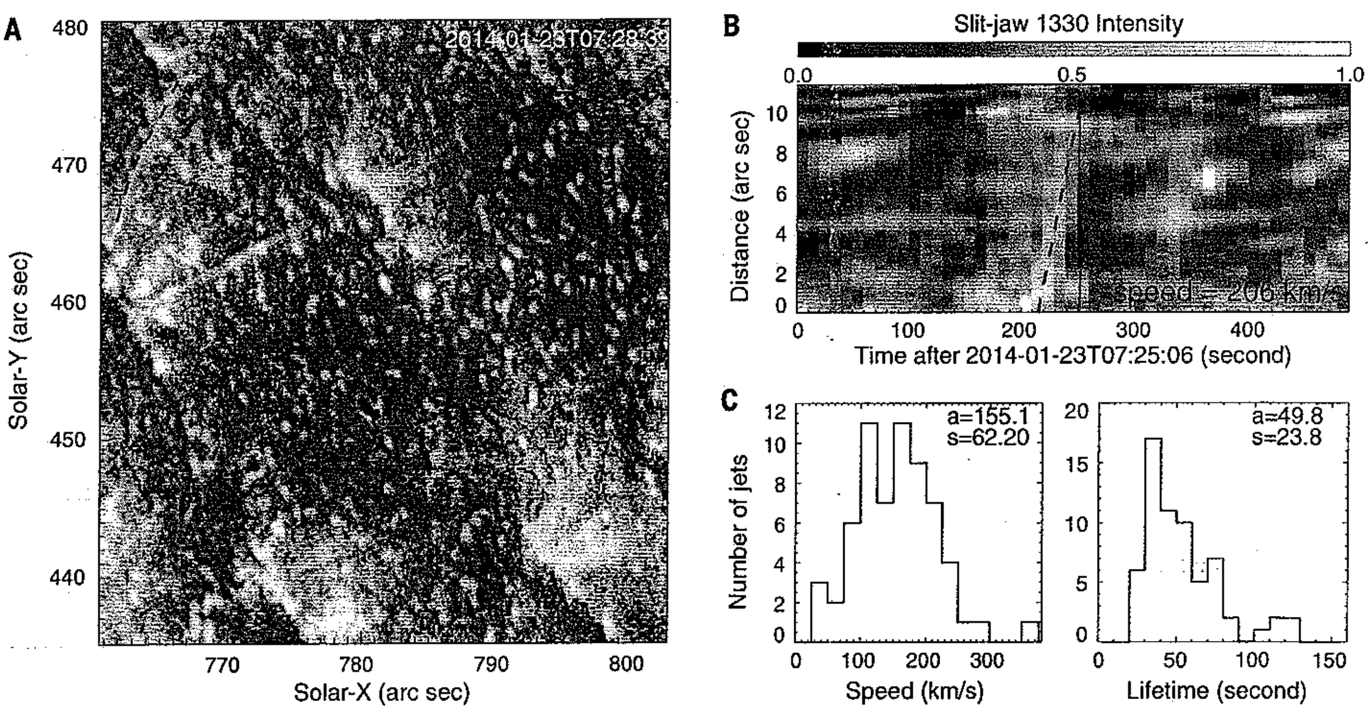

Fig. 1. Examples of network jets. (**A**) An unsharp masked (SM) 1330 Å slit-jaw image (movie S3). The dashed line marks the path of a jet. (**B**) Space-time plot for the jet marked in (A). (**C**) Distributions of the apparent speeds and lifetimes for 63 jets. The average (a) and standard deviation (s) values are also shown.

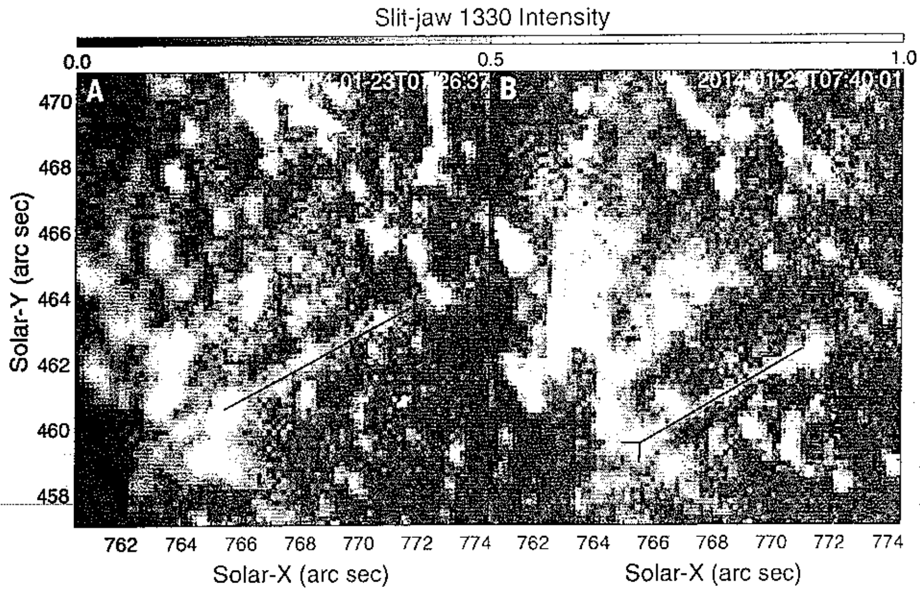

Fig. 2. (A and B) Two unsharp masked 1330 Å slit-jaw images showing the origin of network jets from small-scale bright regions in the network (movie S4). The red lines outline two jets.

of chromospheric upflows being heated to TR temperatures at the solar limb in a coronal hole (*9*).

Using observations from the Interface Region Imaging Spectrograph (IRIS) (*10*), we report results from direct imaging on the solar disk of high-speed upflows with apparent speeds of 80 to 250 km s^{-1}. Thanks to the high resolution (~250 km) in new wavelength windows, IRIS slit-jaw imaging observations with the 1400, 1330, and 2796 Å filters [see the supplementary materials (SM)] unambiguously reveal the prevalence of small-scale jetlike emission features from the bright networks (figs. S1 to S3 and movies S1 and S2). These three filters sample emission from the Si IV, C II, and Mg II ions, which are formed at temperatures of ~10^5 K, ~3 × 10^4 K, and ~10^4 K, respectively. These network jets usually show fast upward motion with no obvious downward component. Although these jets are more easily seen in coronal holes located near the solar limb (movies S1 to S5), they are clearly detected at any location on the solar disk outside active regions (movie S6).

These network jets are best seen in 1330 Å images. The jet widths are usually around ~300 km and approach the instrument resolution limit,

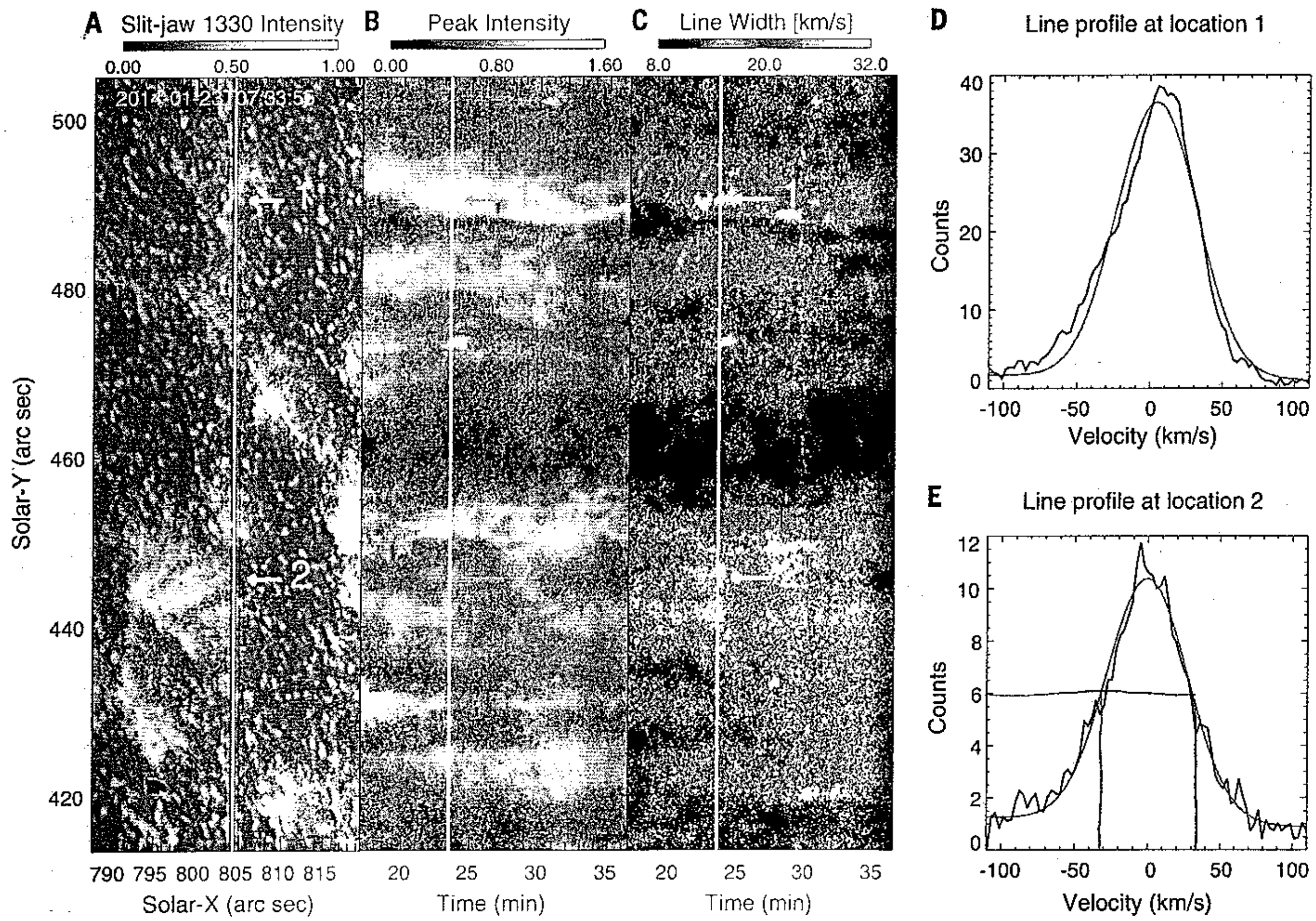

Fig. 3. Signatures of network jets in Si IV 1393.77 Å line profiles (movie S5). (**A**) Unsharp masked 1330 Å slit-jaw image taken at 07:33:55 UT on 23 January 2014. (**B** and **C**) Temporal evolution of the intensity and line width along the slit from a Gaussian fit of Si IV line profiles. The vertical line indicates the slit location in (A) and time of 07:33:55 UT in (B) and (C). (**D** and **E**) Observed line profiles (black) at the two locations indicated by the arrows. Red lines are the Gaussian fits.

suggesting that the actual widths of many jets may be even smaller. By applying the space-time technique (SM) to the 1330 Å image sequence obtained on 23 January 2014 (table S1 and movie S2), we have quantified the apparent speeds and lifetimes for 63 randomly selected jets (Fig. 1). The speeds fall mostly in the range of 80 to 250 km s^{-1}, which is much larger than the sound speed and close to the Alfvén speed in the chromosphere (*11*) and TR. These velocities are significantly larger than previously reported jet velocities in the chromosphere and TR (*12–16*). Some jets also show signatures of acceleration. Their lifetimes range mainly from 20 to 80 s. Most jets extend to lengths of 4 to 10 Mm (1 Mm = 10^6 m), although some clearly reach ~15 Mm.

Many network jets also exhibit obvious motions transverse to their propagation direction, indicating that they carry transverse magnetohydrodynamic waves known as Alfvén waves (*11, 17*). The wave magnitudes are difficult to measure from slit-jaw images, because strong emission from other features complicates the quantification of the transverse displacement, and the jet lifetimes are usually too short to allow the detection of a full wave cycle. Instead, we use spectroscopic observations to estimate the approximate velocity amplitudes of Alfvén waves. The root-mean-square value of the fluctuating Doppler shift of the Si IV 1393.77 Å line is ~5 km s^{-1}, which can be regarded as the resolved wave amplitude (SM and fig. S5).

Many of these network jets are likely the on-disk counterparts and TR manifestation of type II spicules (SM), which are jetlike features moving upward with speeds of 50 to 110 km s^{-1} in the chromosphere above the solar limb (*15, 16*). Our direct imaging of flows along these jets on the solar disk is almost unaffected by line-of-sight superposition, thus providing further support for the debated existence of high-speed jetlike features (*16, 18*). IRIS observations also reveal their origin in the networks, which off-limb observations cannot determine. Yet we notice that network jet velocities are generally twice those of type II spicules, suggesting that the network jets sampled by the TR passbands are those being heated and accelerated in the upper chromosphere and TR (*19*) and/or that the apparent speeds we observe here are not all caused by mass flows. Additional absorbing components at the blue wings of some chromospheric absorption lines were previously claimed to be on-disk counterparts of type II spicules (*13*). These features with speeds of 20 to 50 km s^{-1} are probably the lower-temperature parts and/or less-accelerated phase of the network jets.

Many network jets tend to recur at roughly the same locations on time scales of ~2 to 15 min. Our on-disk observations show that these jets originate from localized bright regions in the networks (Fig. 2 and movie S4). Sometimes we see obvious brightening at the footpoints of these jets. A few jets appear to reveal the characteristic inverted Y-shape morphology (Fig. 2B) that is associated with a bipolar magnetic field line reconnecting with a unipolar large-scale field (*12*). These characteristics, together with the high speeds, suggest that some of these intermittent jets may result from repeated magnetic reconnection (*20*) between small magnetic loops and the background open flux in the networks. It is also possible that the source regions of these jets are too small to be resolved by IRIS, or that other mechanisms (SM) such as flux emergence and the associated Lorentz force are responsible for the acceleration of the jets (*21*).

Spectroscopic observations from IRIS reveal that many jets reach temperatures of at least ~10^5 K, the formation temperature of the Si IV 1393.77 Å line under ionization equilibrium. The most prominent signature of network jets in Si IV line profiles is a significant increase of the line broadening, which could be a consequence of field-aligned flows (*22*) or unresolved transverse motions such as Alfvén waves (*23*) and twists (*24*). Combined imaging and spectral observations of IRIS can help evaluate the contribution from field-aligned flows and transverse motions.

Greatly enhanced widths of the Si IV line are found around two locations of network jets (Fig. 3). The slit crosses the lower part of a recurring jet complex at location 1. There the obvious enhancement of the line profile at the blue wing (Fig. 3D and SM) indicates an association with the network jets visible in the slit-jaw images (movie S5). Thus, the enhanced line broadening here is largely caused by the superposition of the field-aligned flows (jets) on the network background.

Location 2 corresponds to the upper part of some swaying network jets (movie S5). Given the nearly symmetric line profile and that this region is close to the limb, these jets are likely propagating largely in the plane perpendicular to the line of sight. So the line broadening appears to be largely caused by unresolved Alfvén waves, or small-scale twists that are often associated with unresolved torsional Alfvén waves (*25*). If we

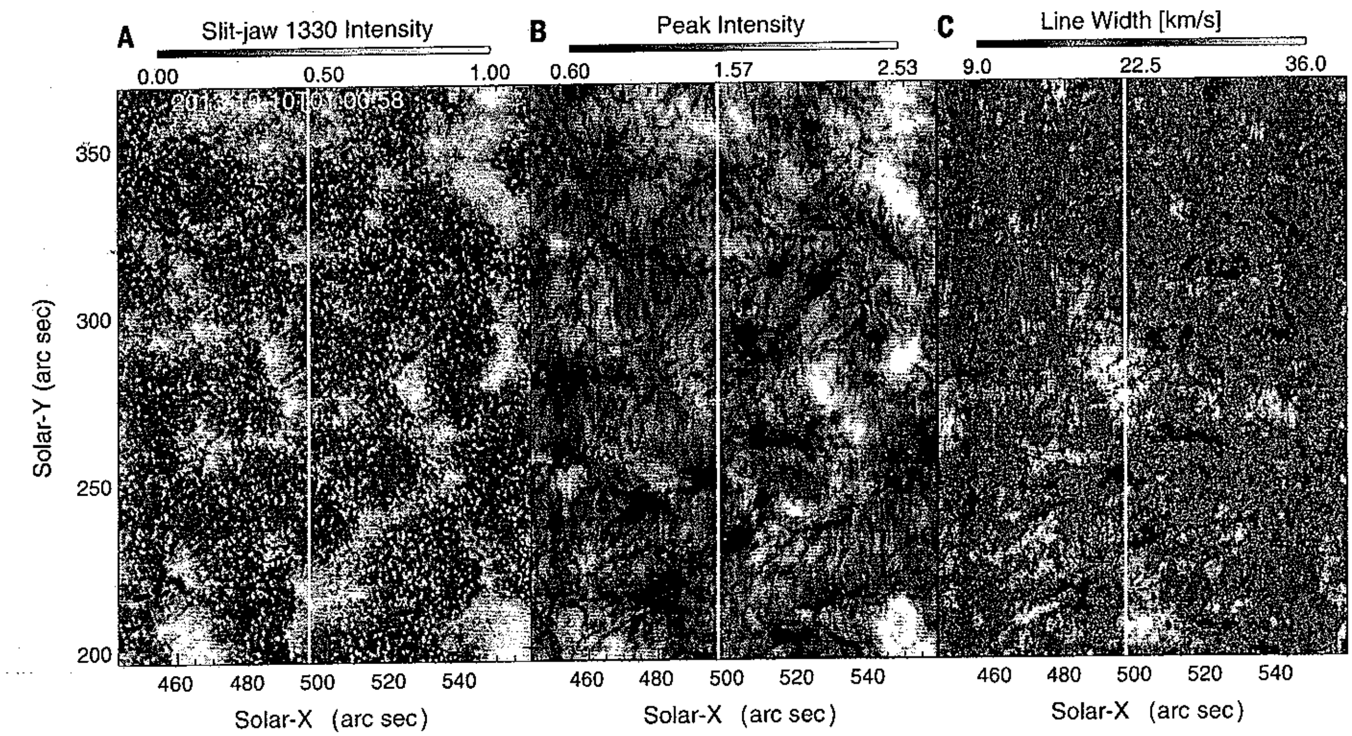

Fig. 4. TR filamentary structures caused by network jets (movie S6). (**A**) An unsharp masked 1330 Å slit-jaw image. (**B** and **C**) Maps of intensity and line width from a Gaussian fit of Si IV 1393.77 Å line profiles. The vertical line indicates the slit location.

attribute the nonthermal width (SM and fig. S5) to these unresolved waves, the wave amplitude is estimated to be ~21 km s^{-1}.

Intensity and linewidth maps of Si IV (Fig. 4) reveal details of the TR structures. One prominent feature of these maps is the presence of filamentary or elongated structures. Comparing these maps with the slit-jaw images (movie S6) reveals an association of many such features with network jets. Depending on viewing angles, enhanced line widths in these filamentary structures could be caused by either the superposition of jet emission on the network background, or unresolved transverse motions, or both. This association reveals that network jets constitute an important element of TR structures (SM).

These jets are likely to be an intermittent but continual source of mass and energy for the solar wind. We find a total mass loss rate of (2.8 to 36.4) × 10^{12} g s^{-1} for these jets if we assume that all jet plasma contributes to the solar wind (SM). This value is about 2 to 24 times larger than the total mass loss rate of the solar wind, yet we have to remember that it is difficult to determine the true contribution to the solar wind without sufficiently sensitive coronal observations. With a wave amplitude of ~20 km s^{-1}, the energy flux of Alfvén waves carried by the jets should be 4 to 24 kW m^{-2} (SM). This is much larger than that required to drive the solar wind (~700 W m^{-2}), yet we do not know how much of this energy is dissipated.

The prevalence of these network jets may challenge current solar wind models. Most time-steady descriptions of the solar wind (*1*, *26*) rely on mass flux driven by evaporation from the upper TR, induced by a combination of downward heat conduction from the corona and local radiative losses (*27*). Although successfully predicting the coronal heating and wind properties at Earth, these models usually produce steady flows of only a few kilometers per second in the chromosphere and TR. Such steady low-speed outflows have never been imaged.

In contrast, our IRIS observations reveal the presence of intermittent high-speed upflows from the networks. If the mass in these jets actually is lost in the solar wind, then models must be updated to account for this highly intermittent component. A proposed reconnection-driven solar wind model (*6*) may be consistent with our observations. This scenario, which involves reconnection between open field lines in the network and surrounding low-lying loops, has been simulated numerically (*28*). However, the maximum outflow velocities produced by this model are only ~30 km s^{-1}, and it is unclear whether the entire mass and energy flux of the wind can be produced in this way (*29*).

If these jets are not the nascent solar wind, at least their interaction with the wind should be considered in solar wind models, because they are the most prominent TR features in the networks where the wind is believed to originate. One recent model does include some upward and downward motions of the TR plasma (*30*). However, these motions have speeds of ~60 km s^{-1} at most, and the jets we observe show much faster upward motions. Obviously, a successful solar wind model must carefully evaluate the mass and energy contributions from these network jets.

REFERENCES AND NOTES

1. S. R. Cranmer, Coronal holes. *Living Rev. Sol. Phys* **6**, 3 (2009). doi: 10.12942/lrsp-2009-3
2. V. H. Hansteen, M. Velli, Solar wind models from the chromosphere to 1 AU. *Space Sci. Rev.* **172**, 89–121 (2012). doi: 10.1007/s11214-012-9887-z
3. E. M. Reeves, The EUV chromospheric network in the quiet Sun. *Sol. Phys.* **46**, 53–72 (1976). doi: 10.1007/BF00157554
4. K. Wilhelm *et al.*, SUMER - Solar Ultraviolet Measurements of Emitted Radiation. *Sol. Phys.* **162**, 189–231 (1995). doi: 10.1007/BF00733430
5. D. M. Hassler *et al.*, Solar wind outflow and the chromospheric magnetic network. *Science* **283**, 810–813 (1999). doi: 10.1126/science.283.5403.810; pmid: 9933156
6. C.-Y. Tu *et al.*, Solar wind origin in coronal funnels. *Science* **308**, 519–523 (2005). doi: 10.1126/science.1109447; pmid: 15845846
7. B. De Pontieu, S. W. McIntosh, V. H. Hansteen, C. J. Schrijver, Observing the roots of solar coronal heating—in the chromosphere. *Astrophys. J.* **701**, L1–L6 (2009). doi: 10.1088/0004-637X/701/1/L1
8. S. W. McIntosh, R. J. Leamon, B. De Pontieu, The spectroscopic footprint of the fast solar wind. *Astrophys. J.* **727**, 7 (2011). doi: 10.1088/0004-637X/727/1/7
9. B. De Pontieu *et al.*, The origins of hot plasma in the solar corona. *Science* **331**, 55–58 (2011). doi: 10.1126/science.1197738; pmid: 21212351
10. B. De Pontieu *et al.*, The Interface Region Imaging Spectrograph (IRIS). *Sol. Phys.* **289**, 2733–2779 (2014). doi: 10.1007/s11207-014-0485-y
11. B. De Pontieu *et al.*, Chromospheric alfvenic waves strong enough to power the solar wind. *Science* **318**, 1574–1577 (2007). doi: 10.1126/science.1151747; pmid: 18063784
12. K. Shibata *et al.*, Chromospheric anemone jets as evidence of ubiquitous reconnection. *Science* **318**, 1591–1594 (2007). doi: 10.1126/science.1146708; pmid: 18063790
13. L. Rouppe van der Voort, J. Leenaarts, B. de Pontieu, M. Carlsson, G. Vissers, On-disk counterparts of type ii spicules in the Ca II 854.2 nm and Hα lines. *Astrophys. J.* **705**, 272–284 (2009). doi: 10.1088/0004-637X/705/1/272
14. H.-S. Ji, W.-D. Cao, P. Goode, Observation of ultrafine channels of solar corona heating. *Astrophys. J.* **750**, L25 (2012). doi: 10.1088/2041-8205/750/1/L25
15. B. De Pontieu *et al.*, *Pub. Astron. Soc. Japan* **59**, S655 (2007).
16. T. M. D. Pereira, B. De Pontieu, M. Carlsson, Quantifying spicules. *Astrophys. J.* **759**, 18 (2012). doi: 10.1088/0004-637X/759/1/18
17. S. W. McIntosh *et al.*, Alfvénic waves with sufficient energy to power the quiet solar corona and fast solar wind. *Nature* **475**, 477–480 (2011). doi: 10.1038/nature10235; pmid: 21796206
18. Y. Z. Zhang *et al.*, Revision of solar spicule classification. *Astrophys. J.* **750**, 16 (2012). doi: 10.1088/0004-637X/750/1/16
19. J. Martínez-Sykora, V. Hansteen, F. Moreno-Insertis, On the origin of the type II spicules: Dynamic three-dimensional mhd simulations. *Astrophys. J.* **736**, 9 (2011). doi: 10.1088/0004-637X/736/1/9
20. V. Archontis, K. Tsinganos, C. Gontikakis, Recurrent solar jets in active regions. *Astron. Astrophys.* **512**, L2 (2010). doi: 10.1051/0004-6361/200913752
21. M. L. Goodman, Acceleration of type 2 spicules in the solar chromosphere. II. Viscous braking and upper bounds on coronal energy input. *Astrophys. J.* **785**, 87 (2014). doi: 10.1088/0004-637X/785/2/87
22. B. De Pontieu, S. W. McIntosh, Quasi-periodic propagating signals in the solar corona: The signature of magnetoacoustic waves or high-velocity upflows? *Astrophys. J.* **722**, 1013–1029 (2010). doi: 10.1088/0004-637X/722/2/1013
23. J. Chae, U. Schuhle, P. Lemaire, SUMER measurements of nonthermal motions: Constraints on coronal heating mechanisms. *Astrophys. J.* **505**, 957–973 (1998). doi: 10.1086/306179
24. B. De Pontieu *et al.*, *Science* **346**, 1255732 (2014).
25. A. A. van Ballegooijen, M. Asgari-Targhi, S. R. Cranmer, E. E. DeLuca, Heating of the solar chromosphere and corona by Alfvén wave turbulence. *Astrophys. J.* **736**, 3 (2011). doi: 10.1088/0004-637X/736/1/3
26. B. Chandran, T. J. Dennis, E. Quataert, S. D. Bale, Incorporating kinetic physics into a two-fluid solar-wind model with temperature anisotropy and low-frequency Alfvén-wave turbulence. *Astrophys. J.* **743**, 197 (2011). doi: 10.1088/0004-637X/743/2/197
27. R. Hammer, Energy balance of stellar coronae. I - Methods and examples. II - Effect of coronal heating. *Astrophys. J.* **259**, 767 (1982). doi: 10.1086/160213
28. L.-P. Yang *et al.*, Injection of plasma into the nascent solar wind via reconnection driven by supergranular advection. *Astrophys. J.* **770**, 6 (2013). doi: 10.1088/0004-637X/770/1/6
29. S. R. Cranmer, A. A. van Ballegooijen, Can the solar wind be driven by magnetic reconnection in the Sun's magnetic carpet? *Astrophys. J.* **720**, 824–847 (2010). doi: 10.1088/0004-637X/720/1/824
30. T. Matsumoto, T. K. Suzuki, Connecting the Sun and the solar wind: The first 2.5-dimensional self-consistent mhd simulation under the Alfvén wave scenario. *Astrophys. J.* **749**, 8 (2012). doi: 10.1088/0004-637X/749/1/8

ACKNOWLEDGMENTS

IRIS is a NASA Small Explorer mission developed and operated by the Lockheed Martin Solar and Astrophysics Laboratory (LMSAL), with mission operations executed at the NASA Ames Research Center and major contributions to downlink communications funded by the Norwegian Space Center (Norway) through a European Space Agency PRODEX contract. This work is supported by NASA contract NNG09FA40C (IRIS), the Lockheed Martin Independent Research Program, European Research Council grant agreement no. 291058, contract 8100002705 from LMSAL to the Smithsonian Astrophysical Observatory, and NASA grant NNX11AO98G. The publicly available IRIS data (including the data used in this study) are archived at http://iris.lmsal.com/data.html.

SUPPLEMENTARY MATERIALS

www.sciencemag.org/content/346/6207/1255711/suppl/DC1
Supplementary Text S1 to S11
Figs. S1 to S5
Table S1
References (*31–64*)
Captions for Movies S1 to S6
Movies S1 to S6

6 May 2014; accepted 22 September 2014
10.1126/science.1255711